Lithospheric Flexural Isostasy Background of the 2017 Ms7.0 Jiuzhaigou Earthquake and Its Implications on Material Extrusion in the Northeastern Bayan Har Block

Minzhang Hu (mzhhu@whu.edu.cn)
Key Laboratory of Earthquake Geodesy, Institute of Seismology, China Earthquake Administration
Yunlong Wu
Key Laboratory of Earthquake Geodesy, Institute of Seismology, China Earthquake Administration
Hongtao Hao
Key Laboratory of Earthquake Geodesy, Institute of Seisnmology, China Earthquake Administraion
Jiapei Wang
Key Laboratory of Earthquake Geodesy, Institute of Seismology, China Earthquake Administration
Jian Wang
Key Laboratory of Earthquake Geodesy, Institute of Seismology, China Earthquake Administration
Zhongya Li
Key Laboratory of Earthquake Geodesy, Institute of Seismology, China Earthquake Administration

Full paper

Keywords: Lithospheric flexural isostasy, Effective elastic thickness, Jiuzhaigou earthquake, tectonics

Posted Date: June 2nd, 2020

DOI: https://doi.org/10.21203/rs.3.rs-31019/v1

Version of Record: A version of this preprint was published at Tectonophysics on January 1st, 2022. See the published version at https://doi.org/10.1016/j.tecto.2022.229209.

Title: Lithospheric flexural isostasy background of the 2017 Ms7.0 Jiuzhaigou earthquake and its implications on material extrusion in the northeastern Bayan Har block

Author #1: Minzhang Hu, Key Laboratory of Earthquake Geodesy, Institute of Seismology, china Earthquake Administration, mzhhu@whu.edu.cn

Author #2: Yunlong Wu, Key Laboratory of Earthquake Geodesy, Institute of Seismology, china Earthquake Administration, yunlongwu@whu.edu.cn

Author #3: Hongtao Hao, Key Laboratory of Earthquake Geodesy, Institute of Seismology, china Earthquake Administration, haoht2004@sina.com

Author #4: Jiapei Wang, Key Laboratory of Earthquake Geodesy, Institute of Seismology, china Earthquake Administration, Wang_jia_pei@163.com

Author #5: Jian Wang, Key Laboratory of Earthquake Geodesy, Institute of Seismology, china Earthquake Administration, kimyin447@163.com

Author #6: Zhongya Li, Key Laboratory of Earthquake Geodesy, Institute of Seismology, china Earthquake Administration, lzy56868@126.com

corresponding author: Minzhang Hu, mzhhu@whu.edu.cn

Abstract: We applied a 2-dimensional, non-spectral technique to investigate the spatial variations of the lithospheric effective elastic thickness (T_e) in the eastern Bayan Har block and its adjacent areas. T_e values were determined by comparison of observed and flexural modelled Bouguer gravity anomalies. The results suggested that T_e vary significantly from eastern Tibet to the Sichuan basin. The eastern Bayan Har block and northern Sichuan-Yunan block had low T_e ($0<T_e<20$km), indicated easily deformable lithosphere. The Sichuan basin had high T_e ($40\text{km}<T_e<100\text{km}$), and acted as a rigid block which resisted the eastward extrusion of plateau materials. Moderate T_e ($30\text{km}<T_e<40\text{km}$) under the Longmen Shan fault belt indicated that the lithosphere of the Sichuan basin plays an important role in supporting the Longmen Shan topography. The extremely low T_e ($T_e<10$km) in the seismogenic zone of the Ms7.0 Jiuzhaigou earthquake indicated that the topography is compensated locally, different from the Longmen Shan significantly. A banded relatively low T_e (<40km) region stretched from northeastern Bayan Har block to southwestern Ordos block sketches out a plateau material escaping channel, questions the exiting of crustal flow in the north side of the Sichuan basin.

Keywords: Lithospheric flexural isostasy, Effective elastic thickness, Jiuzhaigou earthquake, tectonics

Introduction

On August 08, 2017, the Ms7.0 Jiuzhaigou earthquake stroke the northeastern margin of the Bayan Har block. The focal mechanism, distribution of relocated aftershocks and emergency field surveying indicate that the seismogenic fault is a sinistral fault located in the intersection area among the Tazang, Minjiang, and Huya faults (Xu et al., 2017; Liang et al., 2018; Nie et al., 2018; Liu et al., 2019).

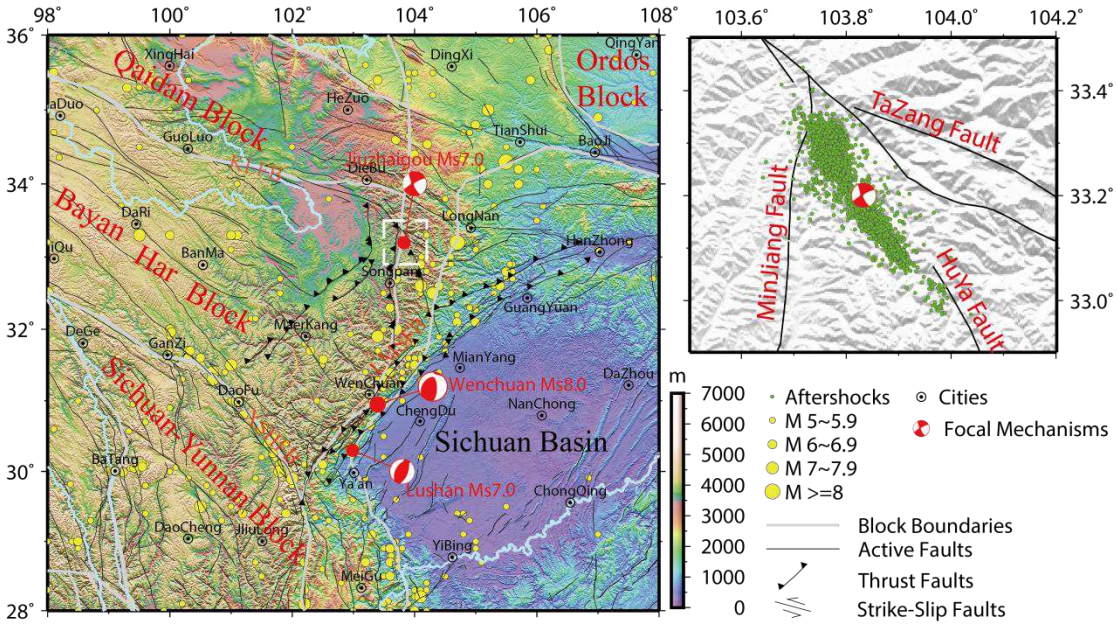

Fig.1 Tectonic settings and distribution of earthquakes in the studied area. The KLFB (Kunlun Fault Belt), LMSFB (Longmen Shan Fault Belt), and XSHFB (Xianshuihe Fault Belt) define the northern, eastern and southern boundaries of the Bayan Har block respectively. The relocated aftershocks (green dots) from Liang et al. (2018) describe the location of the seismogenic fault.

Many geodesy, geological and geophysical measurements have been used to explain the crustal deformation, material extrusion, and high seismicity of the eastern Bayan Har block. GPS observations show that the Qinghai-Tibet plateau is undergoing north-south compression and east-west materials extrusion (Wang et al., 2001; Zhang et al., 2004; Gan et al. 2007). The eastward crustal moving is inhibited by the rigid Sichuan basin, causing crustal thickening and uplifting in eastern Tibet (Liang et al., 2013; Hao et al., 2014). The Kunlun fault notes the north boundary of the Bayan Har block and plays an important role in accommodating Indo-Asian continental collision (Tapponnier and Molnar, 1976; Tapponnier, 2001). Geological surveys suggested that the left-lateral slip rates of the Kunlun fault decrease eastward systematic (Van der Woerd et al., 2000; Harkins et al., 2010; Ren et al., 2013). The

Tazang, Minjiang and Huya faults belong to tail structures at the easternmost end of the Kunlun fault zone and absorbed the slip rates by thrusting, shortening, uplifting and regional rotation. Seismological and magnetotelluric explorations have been conducted to investigate the lithosphere structure and materials extrusion mode of the Qinghai-Tibet plateau (Wang et al., 2015; Wang et al., 2017). Some mechanisms of materials eastward extrusion have been proposed (Tapponnier and Molnar, 1976; Replumaz and Tapponnier, 2003; Royden et al., 1997, 2008; Klemperer, 2006), but the definite mode is still subject to debate.

It is supposed that the lateral lithosphere strength variations play an important role in the tectonic process of the eastern Qinghai-Tibetan plateau (Clark and Royden, 2000; Clark et al., 2005; Cook and Royden, 2008). For example, eastward-moving of the deformable Bayan Har block lithosphere is resisted by the rigid Sichuan basin, causing uplift of the Longmen Shan and accumulates stress on faults, which may generate strong earthquakes. The effective elastic thickness (T_e) is a proxy of the lithosphere strength. Some researchers have estimated the T_e on the Qinghai-Tibetan plateau based on the admittance/coherence spectral techniques or forward modelling methods (Braitenberg et al., 2003; Jordan and Watts, 2005; Chen et al., 2013). There have been few studies involve the details of T_e distribution in eastern Bayan Har block and its adjacent areas, and mainly focus on the Longmen Shan ridge (Jiang and Jin, 2005; Fielding and McKenzie, 2012).

In this paper, we estimate T_e in the focal area of the Ms7.0 Jiuzhaigou earthquake, including the eastern Bayan Har block, based on flexural isostasy analysis of gravity and topography data (Watts, 2001), by 2-dimensional, non-spectral method (Jordan and Watts, 2005). Based on a simple plate model, the Moho flexure loading by the topography is calculated by the finite difference method (Van Wees and Cloetingh,

1994). The Bouguer gravity anomalies from the flexed Moho are calculated, and then the most suitable T_e values were determined by comparison of the calculated and observed Bouguer gravity anomalies. Subsequently, combining T_e with other geophysical data, we discussed the lithospheric isostasy background of the Ms7.0 Jiuzhaigou earthquake and the possible status of materials escaping in the northeastern Bayan Har block.

Theory and method

According to the lithosphere flexural isostasy model, the lithosphere can be described by a simple plate model, which has an elastic plate that lays over a fluid asthenosphere (Watts, 2001). The flexure of the lithosphere can be depicted by Moho undulations. The lithospheric flexure loading under the topography can be presented by differential equation (van Wees and Cloetingh, 1994),

$$\mathrm{D}\frac{\partial^4 \mathrm{w}}{\partial \mathrm{x}^4} + \mathrm{D}\frac{\partial^4 \mathrm{w}}{\partial \mathrm{y}^4} + 2\mathrm{D}\frac{\partial^4 \mathrm{w}}{\partial \mathrm{x}^2\,\partial \mathrm{y}^2} + 2\frac{\partial \mathrm{D}}{\partial \mathrm{x}}\frac{\partial^3 \mathrm{w}}{\partial \mathrm{x}^3} + \frac{\partial^2 \mathrm{D}}{\partial \mathrm{x}^2}\frac{\partial^2 \mathrm{w}}{\partial \mathrm{x}^2} + 2\frac{\partial \mathrm{D}}{\partial \mathrm{y}}\frac{\partial^3 \mathrm{w}}{\partial \mathrm{y}^3} + \frac{\partial^2 \mathrm{D}}{\partial \mathrm{y}^2}\frac{\partial^2 \mathrm{w}}{\partial \mathrm{y}^2}$$

$$+v\frac{\partial^2 \mathrm{D}}{\partial \mathrm{y}^2}\frac{\partial^2 \mathrm{w}}{\partial \mathrm{x}^2} + v\frac{\partial^2 \mathrm{D}}{\partial \mathrm{x}^2}\frac{\partial^2 \mathrm{w}}{\partial \mathrm{y}^2} + 2\frac{\partial \mathrm{D}}{\partial \mathrm{x}}\frac{\partial^3 \mathrm{w}}{\partial \mathrm{x}\,\partial \mathrm{y}^2} + 2\frac{\partial \mathrm{D}}{\partial \mathrm{y}}\frac{\partial^3 \mathrm{w}}{\partial \mathrm{x}^2\,\partial \mathrm{y}} + 2(1-v)\frac{\partial^2 \mathrm{D}}{\partial \mathrm{x}\,\partial \mathrm{y}}\frac{\partial^2 \mathrm{w}}{\partial \mathrm{x}\,\partial \mathrm{y}}$$

$$=\mathrm{q}+\mathrm{d}\rho\mathrm{g}\mathrm{w} + \sigma_{\mathrm{xx}}T_e\frac{\partial^2 \mathrm{w}}{\partial \mathrm{x}^2} + \sigma_{\mathrm{yy}}T_e\frac{\partial^2 \mathrm{w}}{\partial \mathrm{y}^2} + 2\sigma_{\mathrm{xy}}T_e\frac{\partial^2 \mathrm{w}}{\partial \mathrm{x}\,\partial \mathrm{y}} \qquad (1)$$

where the lithospheric flexural rigidity $\mathrm{D} = ET_e^3/12(1-v^2)$, E is Young's modulus, v is Poisson's ratio, w is the lithospheric flexure (depicted by the flexed Moho), the topography loading $\mathrm{q} = \rho_c \mathrm{g} h$, ρ_c is the crustal density, h is topography elevation, g is gravitational acceleration, ρ_m is the mantle density, ρ_{in} is the density of the filled materials, $d\rho = \rho_{in} - \rho_m$, ($\sigma_{\mathrm{xx}}$, σ_{yy}, σ_{xy}) are components of the lateral tectonic stress.

Table 1 Mean Crustal parameters used in this paper

Parameter	Notation	Value

Density of mantle	ρ_m	3270 kg/m^3
Density of crust	ρ_c	2670 kg/m^3
Density of the filled materials	ρ_{in}	2670 kg/m^3
Mean crustal thickness	T_c	30000m
Young's modulus	E	10^{11} N/m^2
Poisson's ratio	v	0.25
Gravitational acceleration	g	9.81 m/s^2

If T_e is assumed to be constant in the analysis window, Eq.(1) can be solved in the frequency domain, and then T_e can be estimated by the admittance/coherence spectral techniques (Watts, 2001; Kirby, et al., 2014). In our study, the finite difference method was used to solve Eq.(1), which can take into account the lateral variation of T_e in the analysis window. Replacing the partial differential formulas using the central difference formulas, the Eq.(1) can be transformed into linear equations,

$$\mathrm{AW} = \mathrm{H} \tag{2}$$

where $\mathrm{W} = (\mathrm{w}_1, \mathrm{w}_2, \cdots \mathrm{w}_\mathrm{i} \cdots \mathrm{w}_{\mathrm{MN}-1}, \mathrm{w}_{\mathrm{MN}})^{\mathrm{T}}$ and $\mathrm{H} = \mathrm{C}_2(h_1, h_2, \cdots h_i \cdots h_{MN-1}, h_{MN})^{\mathrm{T}}$ are column vectors , $\mathrm{C}_2 = \frac{\rho_c g}{\mathrm{D}}\mathrm{dx}^4$, and A is a MN×MN diagonal sparse matrix.

For example, a Gaussian-type mountain with elevation of 2km in the center loading on an elastic plate with variable T_e will introduce Moho flexure, as shown in Fig.2. The Moho flexure (W) is obtained by solving the Eq.(2). The Bouguer gravity anomalies induced from the flexed Moho were calculated by Parker's formula (Parker, 1973). Then the most suitable T_e value was determined by minimizing the root-mean-square (RMS) misfit between the calculated and observed Bouguer gravity anomalies. The iterative strategy proposed by Jordan and Watts (2005) was used to

capture a reasonable spatially distribution of T_e. The results shown in Fig.3 indicate that the T_e structure can be recovered well in the center 200km×200km of the plate. The absolute differences between the inputted and recovered T_e are lower than 2km.

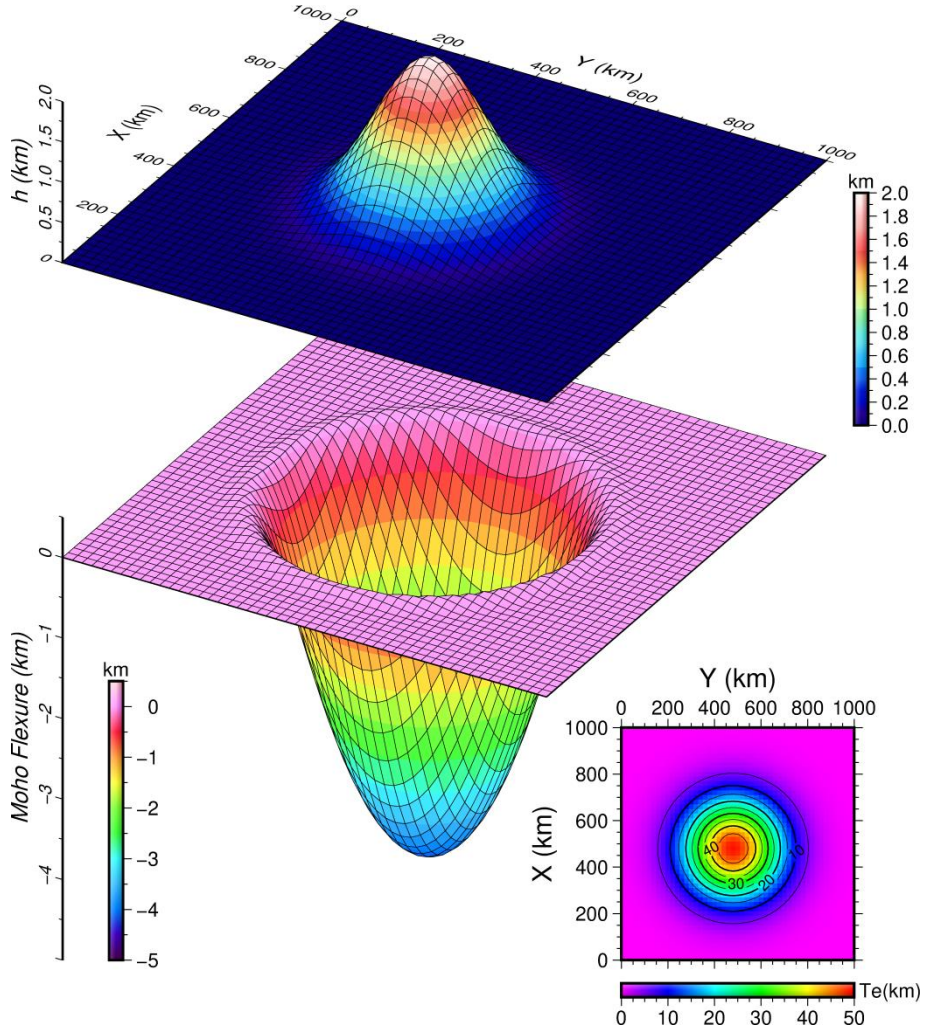

Fig.2 Modelled Gaussian-type mountain with elevation of 2km in the center (upper) loading on an elastic plate with variable Te (lower right corner) , and the introduced Moho flexure (lower).

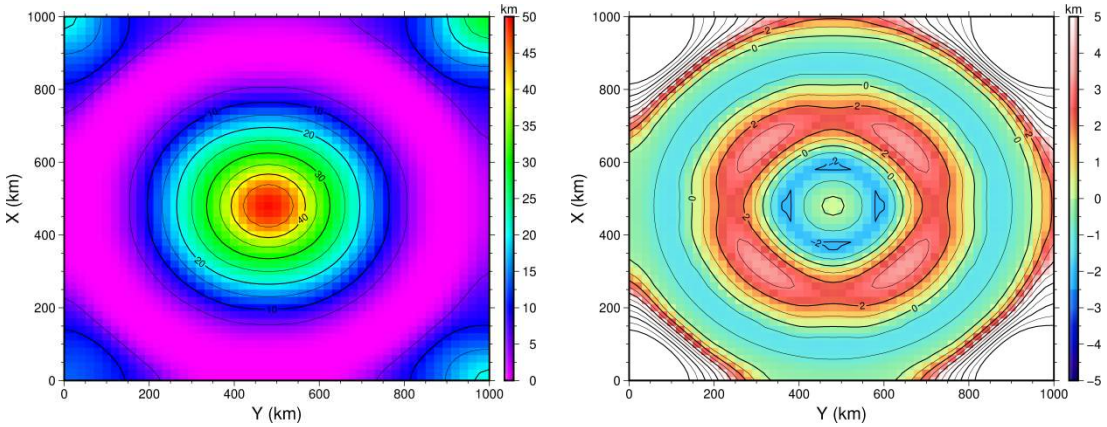

Fig.3 The recovered Te structure (left) and the differences between the inputted and recovered Te (right). The results indicate that the Te structure can be recovered well in the center 200km×200km of the plate, and the absolute differences between the inputted and recovered Te are lower than 2km.

Data and results

Topography and gravity models were used to estimate T_e in this study. The ETOPO1 global relief topography model downloaded from NCEI (National Centers for Environment Information) (Amante and Eakins, 2009) act as loading on the elastic plate, Fig.4. Simple Bouguer gravity anomalies were calculated from the EIGEN6C4 combined gravity model (Förste et al.， 2014), using the online service of the ICGEM (International Center for Global Earth Models), Fig.5. The EIGEN6C4 model has higher quality than EGM2008 at wavelengths longer than 100km, for combining of the GOCE data. A 50km low-pass filter was applied to the downloaded simple Bouguer gravity anomalies, which will suppress the impact of local terrain fluctuation and unreliable short-wavelength fluctuations of the EIGEN6C4 model (Fielding and McKenzie, 2012).

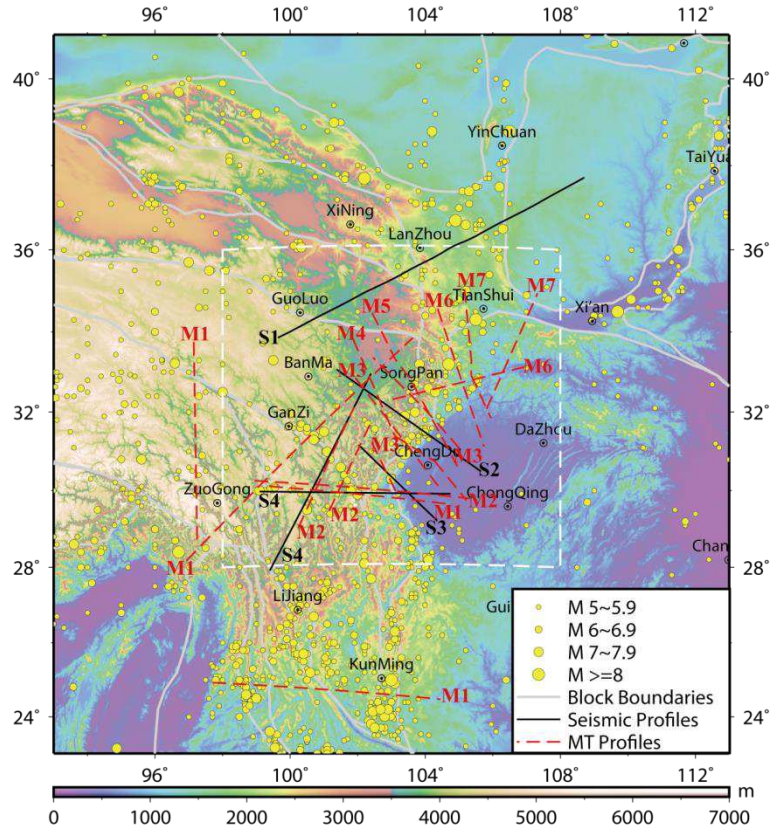

Fig.4 The topography from ETOPO1 in the studied area. T_e was calculated in the white dashed box. S1~S4 are seismic surveying profiles. M1~M7 are magnetotelluric surveying profiles. S1: The Darlag-Lanzhoou-Jingbian seismic refraction profile across the northeastern Qinghai-Tibet Plateau (Liu et al., 2006), S2: The deep seismic wide-angle reflection/refraction profile stretched over the meizoseismal area of the Ms8.0 Wenchuan earthquake, on May 12, 2008 (Jia et al., 2014), S3: The high-resolution wide-angle reflection/refraction profile stretched over the epicentral area of the Ms7.0 Lushan earthquake, on April 20, 2013 (Wang et al., 2015), S4: The deep seismic sounding profiles cross eastern margin of the plateau (Wang et al., 2007). M1: The magnetotelluric profiles extend from the Qinghai-Tibet Plateau into southwest China (Bai et al., 2010), M2: The magnetotelluric sounding profiles from Sun et al.(2003), M3: The magnetotelluric profiles across the LMSFB (Zhao et al., 2012), M4: The Long-period magnetotelluric and broadband magnetotelluric sounding profile across the middle section of LMSFB (Wang et al., 2014), M5: The

Luqu-Zhongjiang magnetotelluric profile from Wang et al. (2009), M6: The magnetotelluric profiles from Min et al.(2017), M7: The magnetotelluric profiles from Zhan et al.(2014).

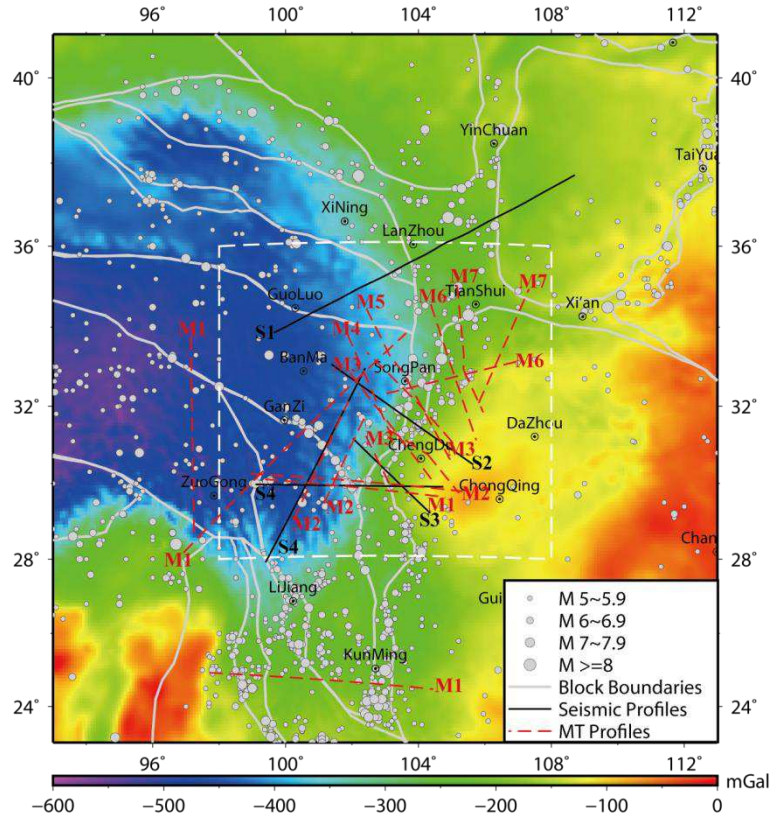

Fig.5 The Bouguer gravity anomalies from EIGEN6C4 in the studied area. S1~S4 are seismic surveying profiles, and M1~M7 are magnetotelluric surveying profiles, the same in Fig.4.

The recovered T_e over the eastern Bayan Har block and its adjacent areas is shown in Fig.6(a), and the calculated Bouguer gravity anomalies are shown in Fig.6(b). Fig.6(a) shows that T_e varies significantly from the eastern margin of the plateau to Sichuan basin. The eastern Bayan Har block and northern Sichuan-Yunan block has low lithospheric strength ($0<T_e<20$km), and the Sichuan basin, acts as a rigid block, has high T_e ($40<T_e<100$km).

The reliability of our T_e structure can be evaluated by considering the crustal isostatic status. Isostatic gravity anomalies are defined as differences between the

observed Bouguer gravity anomalies and the effect of the compensation mass, and will be nearly zero if a suitable isostatic model is applied. Fig.6(c) shows that flexural isostatic gravity anomalies are generally subdued, and with amplitude lower than 20mGal in most of the studied region. For the Airy isostatic model, the topography is compensated locally, equivalent to flexural isostatic model with a T_e of 0km. Fig.6(d) shows that Airy isostatic gravity anomalies are lower than -40mGal in most of the studied region, which means that the Moho is deeper than predicted by Airy model. The most distinct feature of the Airy isostatic anomalies is the positive anomalies that correlate with the LMSFB. The flexural isostatic gravity anomalies (Fig.6(c)) have smaller amplitude than the Airy isostatic gravity anomalies (Fig.6(d)), and show no obvious anomaly features along the block boundaries, which mean that the flexural isostatic model (with variable T_e) is superior to Airy model in the studied area.

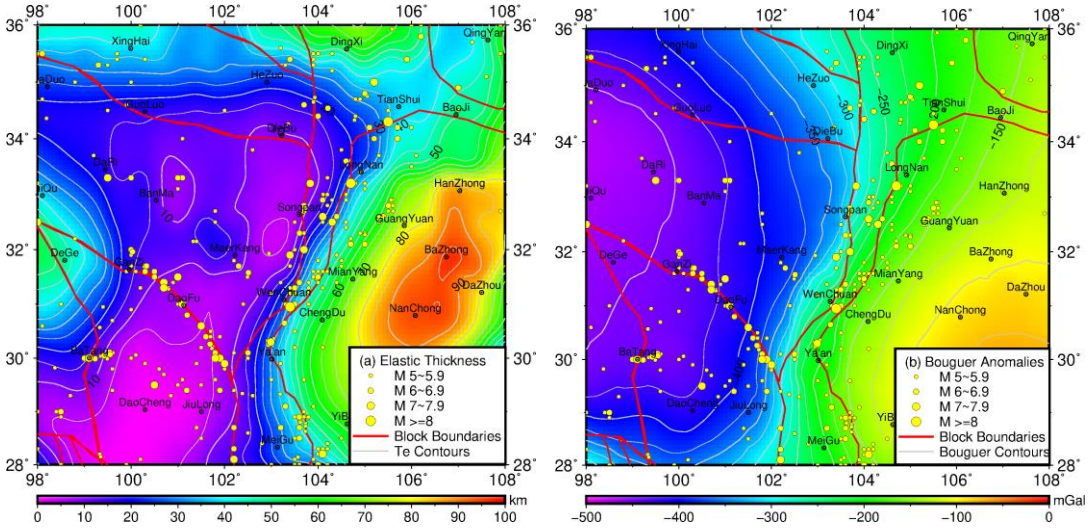

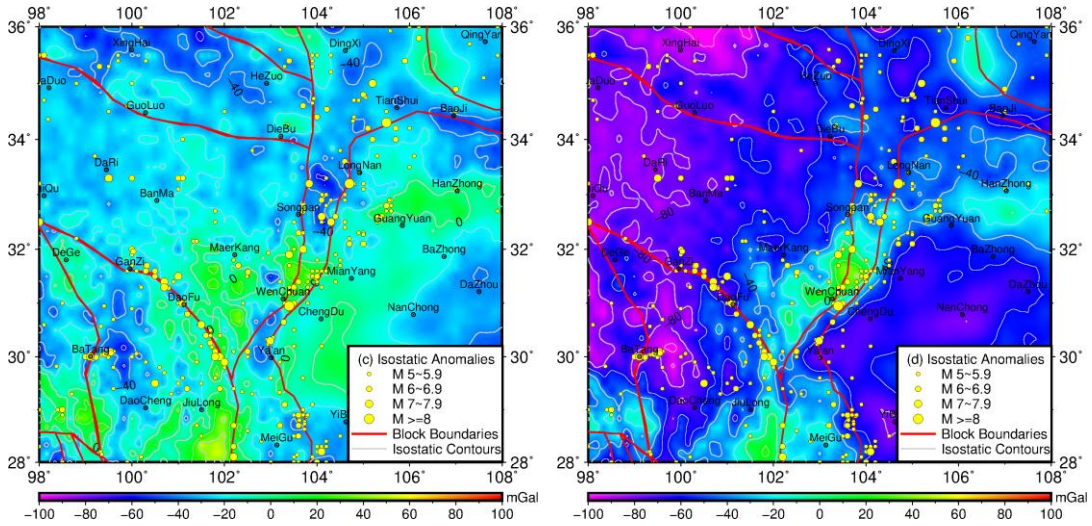

Fig.6 The recovered T_e over the eastern Bayan Har block and its adjacent areas (a), the calculated Bouguer anomalies (b), the flexural isostatic anomalies (c), and the Airy isostatic anomalies (d).

Various authors have investigated the T_e structure over the Qinghai-Tibet plateau and the Sichuan basin. Our estimate of low T_e ($0<T_e<20$km) in the eastern Tibet and high T_e ($40<T_e<100$km) in the Sichuan basin are consistent with some previous results. Braitenberg et al. (2003) suggested low T_e of 10-30km in most of the Tibetan Plateau, including values lower than 10km in the eastern margin of the plateau. Yong et al. (2003) gave T_e of 43-54km in the foreland basin of Longmen Shan by stratigraphy analysis method. Jordan and Watts (2005) suggested a weak ($0<T_e<20$km) lithosphere region extends from the central plateau into south-western China, and T_e is about 50km in western Sichuan basin. Fielding and McKenzie (2012) estimated T_e=54.6km in the Sichuan basin by profile-fitting method, and T_e=7km in eastern Tibet by two-dimensional admittance analysis method. Chen et al. (2013) estimated variations of T_e over China by multitaper coherence analysis of topography and Bouguer gravity anomalies. They suggested high T_e (>60km) in the eastern Sichuan Basin, but low T_e (10-40km) in the west and middle may be due to the dominated effect of the large topography of LMSFB. Jiang and Jin (2005) obtained

212 variable T_e of 36~45km, increasing from the eastern Bayan Har block to western
213 Sichuan basin. This high T_e value (T_e=36km) for eastern Bayan Har block is
214 inconsistent with our results.

215 **Discussions**

216 Our T_e structure revealed a dramatic difference of lithosphere strength from the
217 eastern Tibet to the Sichuan basin. Low T_e ($0<T_e<20$km) region were recovered in
218 eastern Tibet, indicates of long-term deformable lithosphere, correlate well with
219 geodesy and geophysical studies. GPS-derived velocity field showed continuously
220 crustal shortening and uplifting in eastern Tibet (Wang et al., 2001; Zhang et al., 2004;
221 Liang et al., 2013). Seismic and magnetotelluric surveys found broadly distribution of
222 low-velocity and high-conductivity zones in the mid-lower crust of the eastern Tibet
223 (Wang et al., 2015; Wang et al., 2017a), may be due to partial melting of material
224 which will weaken the lithosphere. T_e of LMSFB have moderate values (30-40km),
225 suggested regionally compensation of the large topography. That means the
226 lithosphere of western Sichuan basin plays an important role in supporting the
227 Longmen Shan (Hubbard and Shaw, 2009). Magnetotelluric sounding profile
228 suggested low-conductivity of the lithosphere under the Longmen Shan, that mean
229 lithosphere of western Sichuan basin has wedged into the eastern edge of the Bayan
230 Har block (Wang et al., 2014). The Sichuan basin is a high T_e ($40<T_e<100$km) region,
231 similar to Tarim (110km), Qaidam (70km) basin (Braitenberg et al., 2003), and the
232 Himalaya foreland (40~100km, Jordan and Watts, 2005). Given that the Sichuan basin
233 has Precambrian basement (Ministry of Geology and Mineral Resources, 1991; Chen
234 et al., 1994), high seismic wave velocity (Du et al., 2019), and relatively low heat
235 flow (Jiang et al., 2019), the estimated high T_e values are reasonable. The low T_e in
236 eastern Tibet and high T_e in Sichuan basin revealed in this paper supports the view

237 that eastward extrusion of the deformable plateau materials is resisted by the rigid
238 Sichuan basin (Clark and Royden, 2000; Clark et al., 2005; Cook and Royden, 2008).
239 The Ms7.0 Jiuzhaigou earthquake occurred in the northeastern of Bayan Har
240 block, where has distinctly different isostatic status from LMSFB. Low T_e (<20km)
241 values are recovered in that region, and there are extremely low T_e (<10km) in the
242 seismogenic zone of the Jiuzhaigou earthquake, which means mechanically weak
243 lithosphere consistent with seismic and magnetotelluric tomography results (Du et al.,
244 2019; Riaz et al., 2019; Sun et al., 2020). The T_e structure also suggested that there is
245 a banded low T_e (<40km) region stretched from the northeastern Bayan Har block to
246 the southwestern Ordos block. This low T_e region sketched out a deformable channel,
247 which may support the escape of the plateau material, correlates well with the seismic
248 low-velocity (Liu et al., 2006; Wang et al., 2007; Jia et al., 2014; Wang et al., 2015;
249 Wang et al., 2017b) and high-conductivity zone (Wang et al., 2009; Zhao et al., 2012;
250 Wang et al., 2014; Zhan et al., 2014; Min et al., 2017), Fig.7(a), questions the exiting
251 of crustal flow in the north side of the Sichuan basin. The GPS velocity relative to
252 Southeastern China (Dr. B. Zhao, personal communication) also directed to
253 northeastern in the seismogenic zone, Fig.7(b). The eastward extrusion of materials
254 along the Kunlun fault was not resisted by any rigid blocks in the east but absorbed by
255 crustal thickening, rising, rotation and escaping.

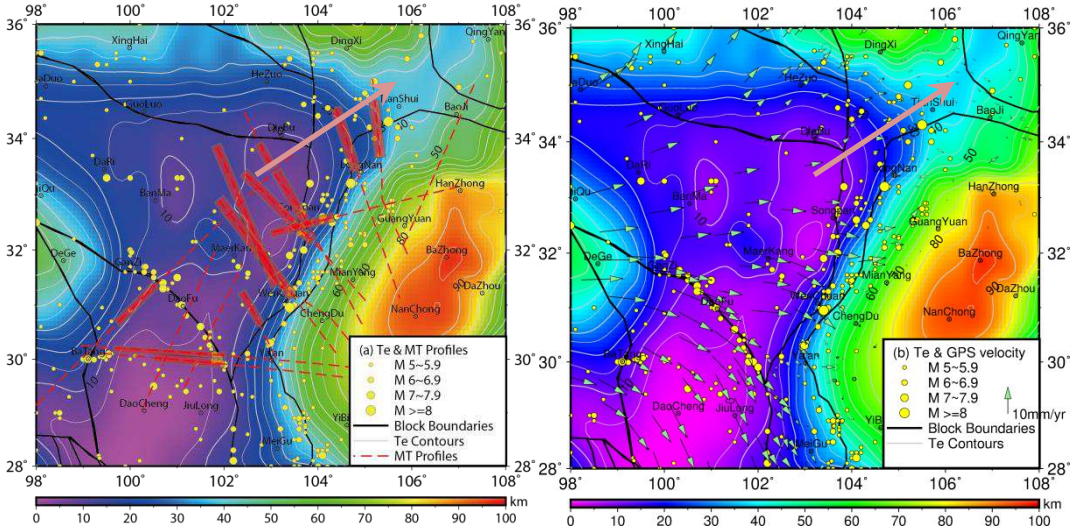

Fig.7 The recovered T_e structure and distribution of the high-conductivity zones on MT profiles (a). The red dashed lines show the same MT profiles in Fig.4. The red shadows on MT profiles indicate high-conductivity zones. The relative low T_e (<40km) region from the northeastern Bayan Har block to southwestern Ordos block correlates well with the high-conductivity zones. The GPS velocity relative to Southeastern China (Dr. B. Zhao, personal communication) also directed to northeastern in the seismogenic zone of the Ms7.0 Jiuzhaigou earthquake (b). The pink arrows indicate possible channel of material extrusion.

Conclusions

1. We revealed T_e structure in the eastern Bayan Har block and its adjacent areas by 2-dimensional, non-spectral analysis of Bouguer gravity anomalies and topography data. The results suggested distinguishable lithosphere strength from eastern Tibet to Sichuan basin.
2. The eastern Tibet is a low T_e ($0<T_e<20$km) region, which means easily deformable lithosphere of the plateau. The Sichuan basin has high T_e ($40<T_e<100$km), similar to previous studies of the Tarim, Qaidam and Himalayan foreland basins, and acts as a rigid block which resisted the eastward extrusion of plateau materials. Moderate strength ($30<T_e<40$km) of the lithosphere under LMSFB suggested that

the lithosphere of the Sichuan basin may play an important role in supporting the thrusting Longmen Shan crust.

3. The seismogenic zone of the Ms7.0 Jiuzhaigou earthquake has extremely low T_e (<10km), and there is a banded low T_e (<40km) region stretched from the northeastern Bayan Har block to the southwestern Ordos block. This low T_e region may sketch out deformable materials escaping channel of the eastward extrusion plateau, questions the exiting of crustal flow in the north side of the Sichuan basin.

Availability of data and materials

The data that support the findings of this study are available upon reasonable request to Minzhang Hu. (email: mzhhu@whu.edu.cn)

Abbreviations

LMSFB: Longmen Shan Fault Belt; GPS: Global Positioning System; NCEI: National Centers for Environment Information; ICGEM: International Center for Global Earth Models.

Authors' contributions

Minzhang Hu calculated the T_e and drafted the manuscript. Yunlong Wu tested the program and made the example in Fig.2 and Fig.3. Hongtao Hao analyzed the relationship between T_e and seismic low-velocity zones. Jiapei Wang analyzed the relationship between T_e and magnetotelluric high-conductivity zones. Jian Wang discussed the distribution of T_e and its means to material extrusion of the plateau. Zhongya Li analyzed the relationship between T_e and GPS velocity. All authors read and approved the final manuscript.

Acknowledgements

We are grateful to the NCEI and ICGEM for providing free topography and gravity model data. Generic Mapping Tools (GMTs) provided by Wessel and Smith(1998) were used to develop the figures. We are thankful to Dr. B. Zhao for providing GPS velocity data in Fig.7(b) and S.S. Liang for providing relocated aftershocks in Fig.1. We thank the anonymous reviewers and the editor for their helpful comments to

improve our manuscript.

Ethics approval and consent to participate

Not applicable.

Competing interests

The authors declare that they have no competing interests.

Funding

This research was supported by the National Natural Science Foundation of China (Grant No.41974021, 41931074，41974096), the Science for Earthquake Resilience of China Earthquake Administration (XH20039) and National Key R&D Program of China (Grant No.2018YFC1503503-01).

Publisher's Note

Springer Nature remains neutral with regard to jurisdictional claims in published maps and institutional affiliations.

References

Amante C, Eakins BW. (2009) ETOPO1 1 Arc-minute Global Relief Model: Procedures, Data Sources and Analysis. NOAA Technical Memorandum NESDIS NGDC-24.

Bai DH, Unsworth MJ, Meju MA et al. 2010. Crustal deformation of the eastern Tibetan plateau revealed by magnetotelluric imaging. Nature Geoscience, 3(5): 358-362.

Braitenberg C, Wang Y, Fang J et al. (2003) Spatial variations of flexure parameters over the Tibet-Qinghai plateau. Earth and Planetary Science Letters, 205(3-4):

211-224.

Chen B, Chen C, Kaban MK et al. (2013) Variations of the effective elastic thickness over China and surroundings and their relation to the lithosphere dynamics. Earth and Planetary Science Letters. 363: 61-72.

Chen SF, Wilson CJL, Luo ZL et al. (1994) The evolution of the Longmen Shan foreland basin. J. Southeast Asian Earth Sci, 10: 159-186.

Clark MK, Royden LH. (2000) Topographic ooze: building the eastern margin of Tibet by lower crustal flow. Geology, 28(8): 703-706.

Clark MK, Bush JWM, Royden LH. (2005) Dynamic topography produced by lower crustal flow against rheological strength heterogeneities bordering the Tibetan Plateau. Geophysical Journal International, 162(2): 575-590.

Cook KL, Royden LH. (2008) The role of crustal strength variations in shaping orogenic plateaus, with application to Tibet. Journal of Geophysical Research, 113(B08407), doi:10.1029/2007JB005457.

Du GB, Wu QJ, Zhang XM et al. (2019) Pn wave velocity and anisotropy underneath the central segment of the North-South Seismic Belt in China. Journal of Asian Earth Sciences. 184: 103941.

Fielding EJ, McKenzie D. (2012) Lithospheric flexure in the Sichuan Basin and Longmen Shan at the eastern edge of Tibet. Geophysical Research Letters, 39(9): L09311, doi: 10.1029/2012GL051680.

Förste C, Bruinsma SL, Abrikosov O et al. (2014) EIGEN-6C4：The latest combined global gravity field model including GOCE data up to degree and order 2190 of GFZ Potsdam and GRGS Toulouse. GFZ Data Services, doi: 10.5880/ICGEM.2015.1

Gan WJ, Zhang PZ, Shen ZK et al. (2007) Present-day crustal motion within the

359 Tibetan Plateau inferred from GPS measurements. Journal of Geophysical
360 Research: Solid Earth, 112(B8): B08416, doi: 10.1029/2005JB004120.
361 Hao M, Wang QL, Shen ZK et al. (2014) Present day crustal vertical movement
362 inferred from precise leveling data in eastern margin of Tibetan plateau.
363 Tectonophysics, 632: 281-292.
364 Harkins N, Kirby E, Shi X et al. (2010) Millennial slip rates along the eastern Kunlun
365 fault: Implications for the dynamics of intracontinental deformation in Asia.
366 Lithosphere, 2(4):247-266.
367 Hubbard J, Shaw JH et al. (2009) Uplift of the Longmen Shan and Tibetan plateau,
368 and the 2008 Wenchuan (M=7.9) earthquake. Nature, 458,
369 doi:10.1038/nature07837.
370 Jia SX, Liu BJ, Xu ZF et al. (2014) The crustal structures of the central Longmenshan
371 along and its margins as related to the seismotectonics of the 2008 Wenchuan
372 Earthquake. Science China Earth Sciences, 57(4): 777-790.
373 Jiang GZ, Hu SB, Shi YZ et al. (2019) Terrestrial heat flow of continental China:
374 Updated dataset and tectonic implications. Tectonophysics, 753: 36-48.
375 Jiang XD, Jin Y. (2005) Mapping the deep lithospheric structure beneath the eastern
376 margin of the Tibetan Plateau from gravity anomalies. Journal of Geophysical
377 Research, 110(B07407), doi:10.1029/2004JB003394.
378 Jordan TA, Watts AB. (2005) Gravity anomalies, flexure and the elastic thickness
379 structure of the India-Eurasia collisional system. Earth and Planetary Science
380 Letters, 236(3-4): 732-750.
381 Kirby JF. (2014) Estimation of the effective elastic thickness of the lithosphere using
382 inverse spectral methods: the state of the art. Tectonophysics, 631: 87-116.
383 Klemperer S L. (2006) Crustal flow in Tibet: geophysical evidence for the physical

state of Tibetan lithosphere, and inferred patterns of active flow. Geological Society, London, Special Publications, 268(1): 39.

Liang SM, Gan WJ, Shen CZ et al. (2013) Three-dimensional velocity field of present-day crustal motion of the Tibetan Plateau derived from GPS measurements. Journal of Geophysical Research: Solid Earth, 118(10): 5722-5732.

Liang SS, Lei JS, Xu ZG et al. (2018) Relocation of aftershocks of the 2017 Jiuzhaigou, Sichuan, Ms7.0 earthquake and inversion for focal mechanism of the mainshock. Chin J Geophys. 61(5): 2163-2175. (in Chinese with English abstract)

Liu G, Xiong W, Wang Q et al. (2019) Source characteristics of the 2017 Ms7.0 Jiuzhaigou, China, earthquake and implications for recent seismicity in eastern Tibet. Journal of Geophysical Research: Solid Earth, 124. https://doi.org/10.1029/2018JB016340

Liu MJ, Mooney WD, Li SL et al. (2006) Crustal structure of the mortheastern margin of the Tibetan plateau from the Songpan-ganzi terrane to the Ordos basin. Tectonophysics, 420: 253-266.

Min G, Wang XB, Xia SB et al. (2017) Electrical structure of middle and upper crust beneath the Minshan uplift zone and central section of the West Qinling orogenic zone. Chin J Geophys. 60(6): 2397-2413. (in Chinese with English abstract)

Ministry of Geology and Mineral Resources (1991) Regional geology of Sichuan province, 728 pp., Geol. Publ. House, Beijing.

Nie ZS, Wang DJ, Jia ZG et al. (2018) Fault model of the 2017 Jiuzhaigou Mw6.5 earthquake estimated from coseismic deformation observed using Global Positioning System and Interferometric Synthetic Aperture Radar data. Earth, Planets and Space. 70:55, https://doi.org/10.1186/s40623-018-0826-4.

409 Parker RL. (1973) The Rapid Calculation of Potential Anomalies. Geophys. J.R.
410 Astr.Soc. 31: 447-455.
411 Ren JJ, Xu XW, Yeats RS et al. (2013) Latest quaternary paleoseismology and slip
412 rates of the Longriba fault zone, eastern Tibet: Implications for fault behavior and
413 strain partitioning. Tectonics, 32: 216-238.
414 Replumaz A, Tapponnier P. (2003) Reconstruction of the deformed collision zone
415 between India and Asia by backward motion of lithospheric blocks. Journal of
416 Geophysical Research: Solid Earth, 108(B6): 2285, doi: 10.1029/2001JB000661.
417 Riaz MS, Zheng Y, Liu F et al. (2019) Tomographic imaging of the 2017 Ms7.0
418 Jiuzhaigou earthquake source region and its implications on material extrusion in
419 the northeast Tibetan plateau. Tectonophysics, 752:24-34.
420 Royden LH, Burchfiel BC, King RW et al. (1997) Surface deformation and lower
421 crustal flow in eastern Tibet. Science, 276(5313): 788-790.
422 Royden LH, Burchfiel BC, Van Der Hilst RD. (2008) The Geological evolution of the
423 Tibetan Plateau. Science, 321(5892): 1054-1058.
424 Sun J, Jin GW, Bai DH et al. (2003) Sounding of electrical structure of the crust and
425 upper mantle along the eastern border of Qinghai-Tibet Plateau and its tectonic
426 significance. Science in China (Series D), 46(Supp.): 243-253.
427 Sun XY, Zhan Y, Zhang HP et al. (2020) 3-D magnetotelluric imaging of the
428 easternmost Kunlun fault: insights into strain partitioning and the seismotectonics
429 of the Jiuzhaigou Ms7.0 earthquake. Journal of Geophysical Research: Solid Earth,
430 doi:10.1029/2020JB019731.
431 Tapponnier P, Molnar P. (1976) Slip-line field theory and large-scale continental
432 tectonics. Nature, 264(25): 319-324.
433 Tapponnier P, Xu ZQ, Roger F et al. (2001) Oblique stepwise rise and growth if the

Tibet plateau. Science, 294(5547): 1671-1677.

Van der Woerd J, Ryerson FJ, Tapponnier P et al. (2000) Uniform slip-rate along the Kunlun fault: Implications for seismic behavior and large-scale tectonics. Geophysical Research Letters, 27(16): 2353-2356.

Van Wees JD, Cloetingh S. (1994) A finite-difference technique to incorporate spatial variations in rigidity and planar faults into 3-D models for lithospheric flexure. Geophysical Journal International, 117(1): 179-195.

Wang CY, Han WB, Wu JP et al. (2007) Crustal structure beneath the eastern margin of the Tibetan Plateau and its tectonic implications. Journal of Geophysical Research, 112(B07307), doi:10.1029/2005JB003873.

Wang CY, Yang WC, Wu JP et al. (2015) Study on the lithospheric structure and earthquakes in North-South tectonic belt. Chin J Geophys. 58(11): 3867-3901, doi: 10.6038/cjg20151101. (in Chinese with English abstract)

Wang Q, Zhang PZ, Freymueller JT et al. (2001) Present-day crustal deformation in china constrained by global positioning system measurements. Science, 294(5542): 574-577.

Wang SJ, Wang FY, Zhang JS et al. (2015) The deep seismogenic environment of Lushan Ms7.0 earthquake zone revealed by a wide-angle reflection/refraction seismic profile. Chin J Geophys. 58(9): 3193-3204. (in Chinese with English abstract)

Wang XB, Zhu YT, Zhao XK et al. (2009) Deep conductivity characteristics of the Longmen Shan, eastern Qinghai-Tibet plateau. Chin J Geophys. 52(2): 564-571. (in Chinese with English abstract)

Wang XB, Zhang G, Fang H et al. (2014) Crust and upper mantle resistivity structure at middle section of Longmenshan, eastern Tibetan plateau. Tectonophysics,

619-620: 143-148.

Wang XB, Yu N, Gao S et al. (2017a) Research progress in research on electrical structure of crust and upper mantle beneath the eastern margin of the Tibetan plateau. Chin J Geophys. 60(6): 2350-2370. (in Chinese with English abstract)

Wang XC, Li YH, Ding ZF et al. (2017b) Three-dimensional lithospheric S wave velocity model of the NE Tibetan Plateau and western North China Craton. Journal of Geophysical Research: Solid Earth, doi: 10.1002/2017JB014203.

Watts AB. (2001) Isostasy and Flexure of the Lithosphere. Cambridge: Cambridge University Press.

Xu XW, Chen GH, Wang QX et al. (2017) Discussion on seismogenic structure of Jiuzhaigou earthquake and its implication for current strain state in the southeastern Qinghai-Tibet Plateau. Chin J Geophys. 60(10): 4018-4026. (in Chinese with English abstract)

Yong L, Allen PA, Densmore AL et al. (2003) Evolution of the Longmen Shan foreland basin (Western Sichuan, China) during the Late Triassic Indosinian Orogeny. Basin Research, 15: 117-138.

Zhao GZ, Unsworth MJ, Zhan Y et al. (2012) Crustal structure and rheology of the Longmenshan and Wenchuan Mw7.9 earthquake epicentral area from magnetotelluric data. 40(12): 1139-1142.

Zhan Y, Zhao GZ, Wang LF et al. (2014) Deep electric structure beneath the intersection area of West Qinling orogenic zone with North-South Seismic tectonic zone in China. Chin J Geophys. 57(8): 2594-2607. (in Chinese with English abstract)

Zhang PZ, Shen ZK, Wang M et al. (2004) Continuous deformation of the Tibetan plateau from global positioning system data. Geology, 32(9): 809-812.

Figures

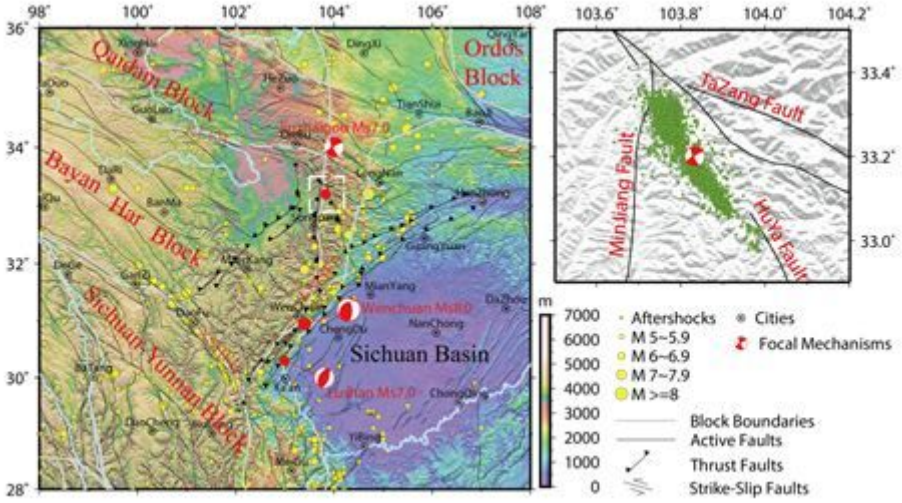

Figure 1

Tectonic settings and distribution of earthquakes in the studied area. The KLFB (Kunlun Fault Belt), LMSFB (Longmen Shan Fault Belt), and XSHFB (Xianshuihe Fault Belt) define the northern, eastern and southern boundaries of the Bayan Har block respectively. The relocated aftershocks (green dots) from Liang et al. (2018) describe the location of the seismogenic fault.

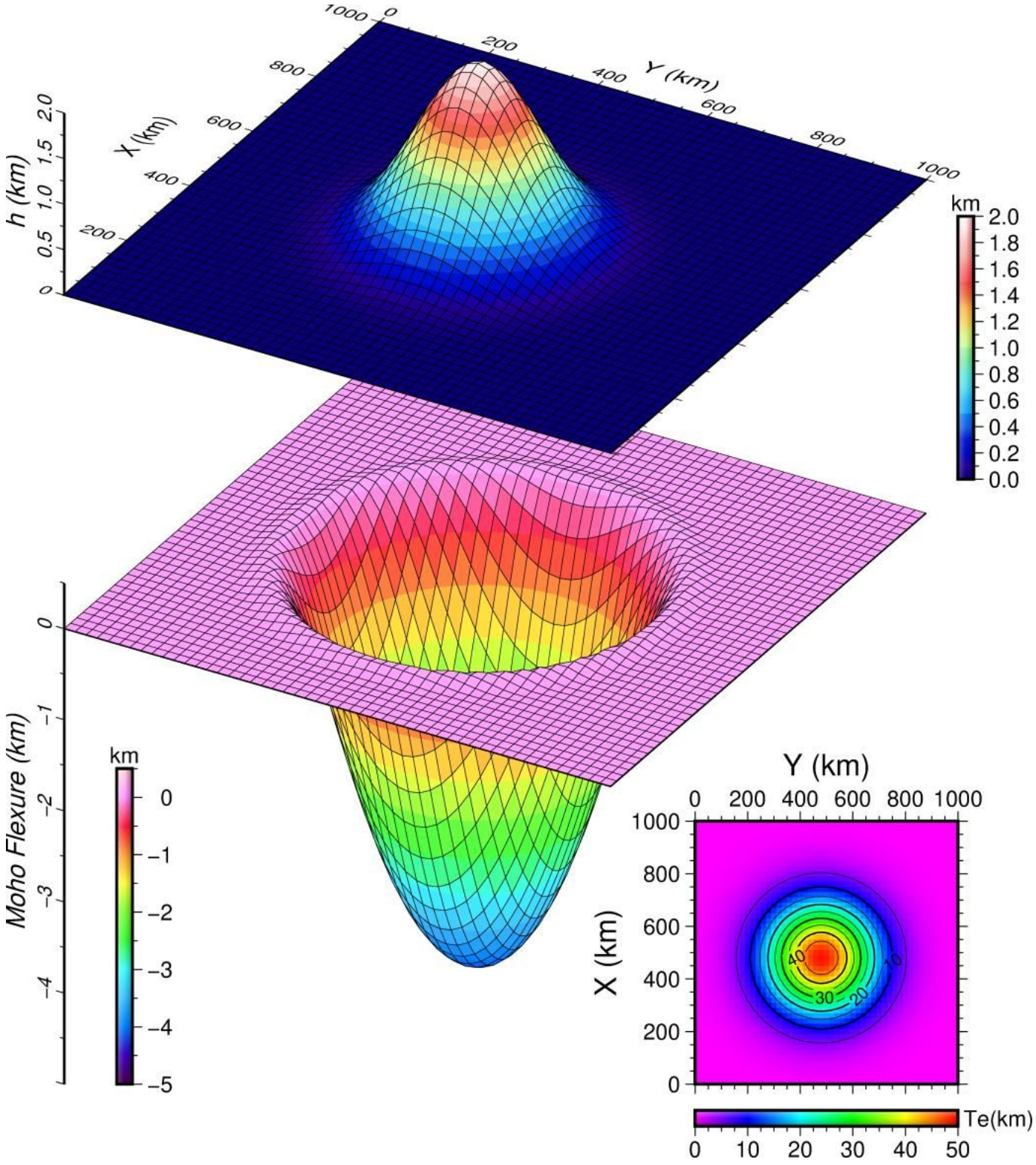

Figure 2

Modelled Gaussian-type mountain with elevation of 2km in the center (upper) loading on an elastic plate with variable Te (lower right corner) , and the introduced Moho flexure (lower).

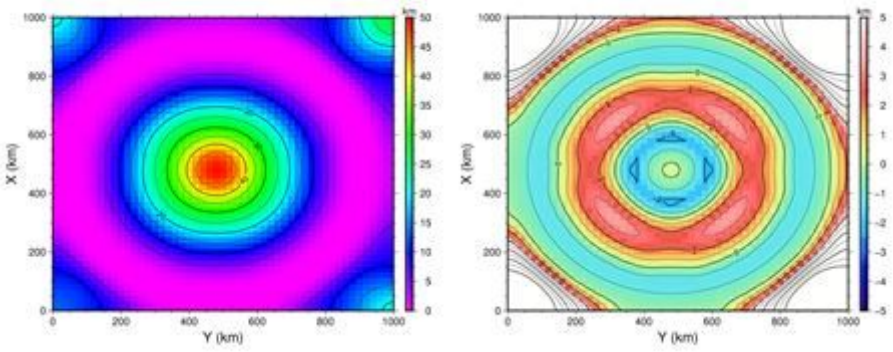

Figure 3

The recovered Te structure (left) and the differences between the inputted and recovered Te (right). The results indicate that the Te structure can be recovered well in the center 200km×200km of the plate, and the absolute differences between the inputted and recovered Te are lower than 2km.

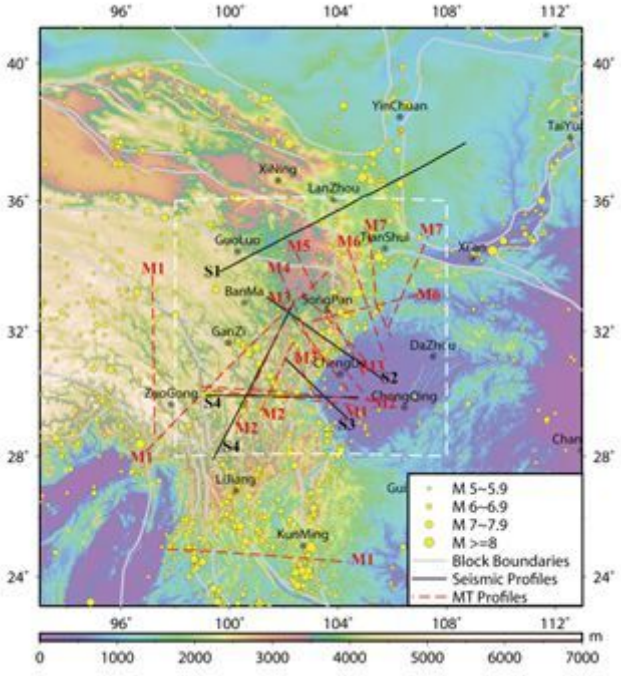

Figure 4

The topography from ETOPO1 in the studied area. Te was calculated in the white dashed box. S1~S4 are seismic surveying profiles. M1~M7 are magnetotelluric surveying profiles. S1: The Darlag-Lanzhoou-Jingbian seismic refraction profile across the northeastern Qinghai-Tibet Plateau (Liu et al., 2006), S2: The deep seismic wide-angle reflection/refraction profile stretched over the meizoseismal area of the Ms8.0 Wenchuan earthquake, on May 12, 2008 (Jia et al., 2014), S3: The high-resolution wide-angle reflection/refraction profile stretched over the epicentral area of the Ms7.0 Lushan earthquake, on April 20, 2013 (Wang et al., 2015), S4: The deep seismic sounding profiles cross eastern margin of the plateau (Wang et al., 2007). M1: The magnetotelluric profiles extend from the Qinghai-Tibet Plateau into southwest China (Bai et al., 2010), M2: The magnetotelluric sounding profiles from Sun et al.(2003), M3:

The magnetotelluric profiles across the LMSFB (Zhao et al., 2012), M4: The Long-period magnetotelluric and broadband magnetotelluric sounding profile across the middle section of LMSFB (Wang et al., 2014), M5: The Luqu-Zhongjiang magnetotelluric profile from Wang et al. (2009), M6: The magnetotelluric profiles from Min et al.(2017), M7: The magnetotelluric profiles from Zhan et al.(2014).

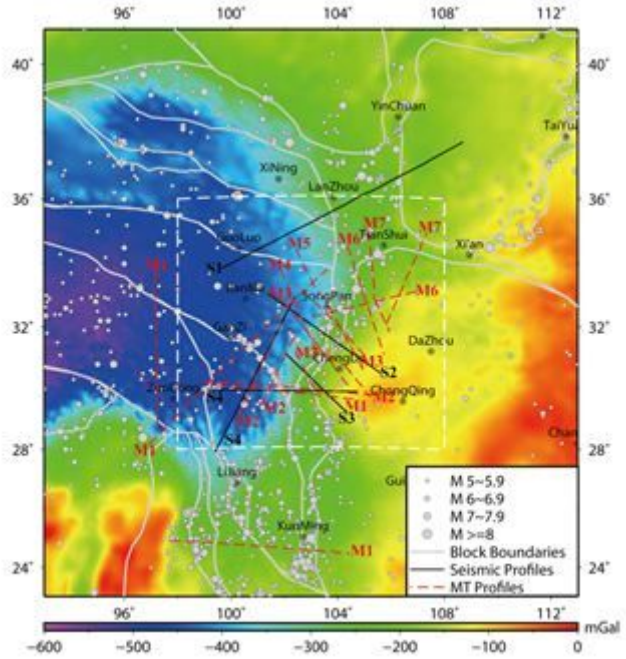

Figure 5

The Bouguer gravity anomalies from EIGEN6C4 in the studied area. S1~S4 are seismic surveying profiles, and M1~M7 are magnetotelluric surveying profiles, the same in Fig.4.

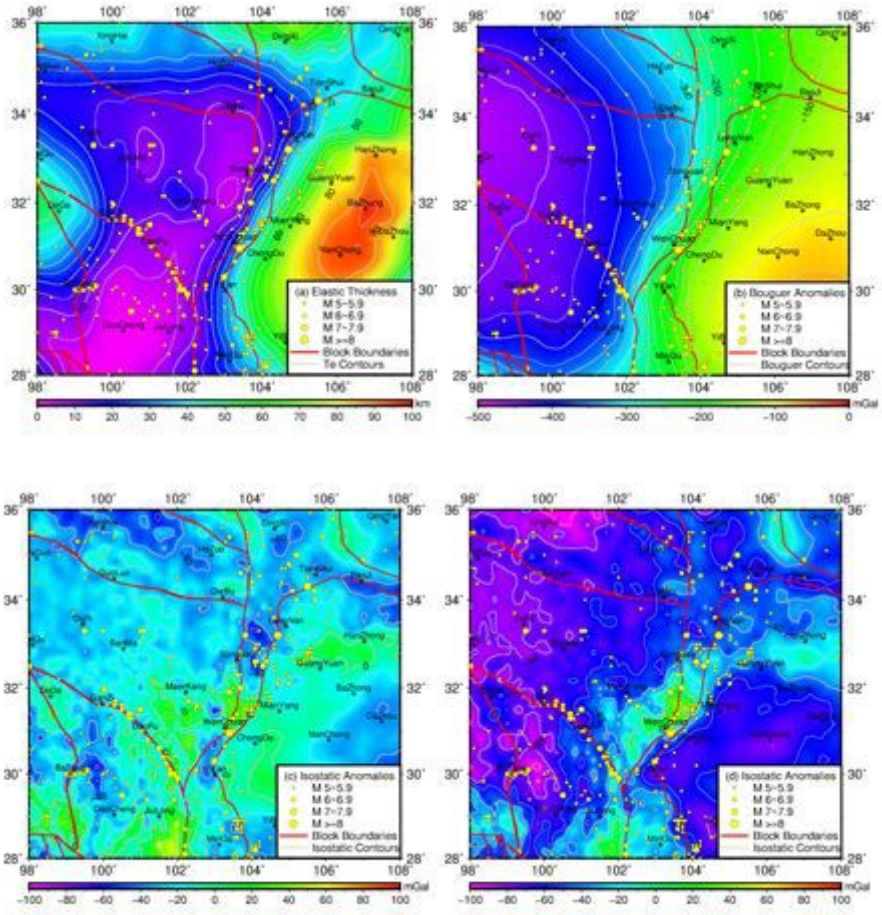

Figure 6

The recovered Te over the eastern Bayan Har block and its adjacent areas (a), the calculated Bouguer anomalies (b), the flexural isostatic anomalies (c), and the Airy isostatic anomalies (d).

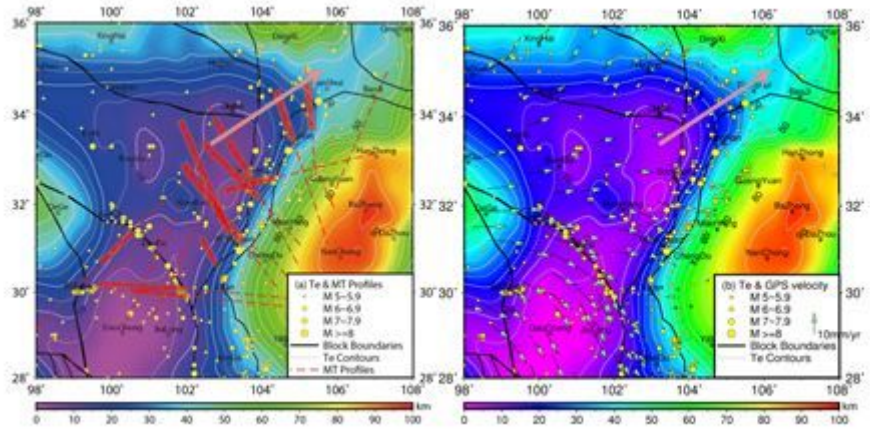

Figure 7

The recovered Te structure and distribution of the high-conductivity zones on MT profiles (a). The red dashed lines show the same MT profiles in Fig.4. The red shadows on MT profiles indicate high-

conductivity zones. The relative low Te (<40km) region from the northeastern Bayan Har block to southwestern Ordos block correlates well with the high-conductivity zones. The GPS velocity relative to Southeastern China (Dr. B. Zhao, personal communication) also directed to northeastern in the seismogenic zone of the Ms7.0 Jiuzhaigou earthquake (b). The pink arrows indicate possible channel of material extrusion.

Supplementary Files

This is a list of supplementary files associated with this preprint. Click to download.

- GraphicalAbstract1.png
- GraphicalAbstract.svg